Magnetic Assembly and Cross-Linking of Nanoparticles for Releasable Magnetic Microstructures

Camilo Velez,[†,‡] Isaac Torres-Díaz,[#,‡] Lorena Maldonado-Camargo,[§,‡] Carlos Rinaldi,[*,#,§] and David P. Arnold[*,†]

[†]Department of Electrical & Computer Engineering, [#]J. Crayton Pruitt Family Department of Biomedical Engineering, and [§]Department of Chemical Engineering, University of Florida, Gainesville, Florida 32611, United States. [‡]C. Velez, I. Torres-Diaz, and L. Maldonado-Camargo contributed equally.

ABSTRACT This article describes a versatile method to fabricate magnetic microstructures with complex two-dimensional geometric shapes using magnetically assembled iron oxide (Fe_3O_4) and cobalt ferrite ($CoFe_2O_4$) nanoparticles. Magnetic pole patterns are imprinted into magnetizable media, onto which magnetic nanoparticles are assembled from a colloidal suspension into defined shapes *via* the shaped magnetic field gradients. The kinetics of this assembly process are studied by evaluation of the microstructure features (*e.g.*, line width and height) as a function of time, particle type, and volume fraction. After assembly, the iron oxide particles are cross-linked *in situ* and subsequently released by dissolving a sacrificial layer. The free-floating magnetic structures are shown to retain their patterned shape during manipulation with external magnetic fields.

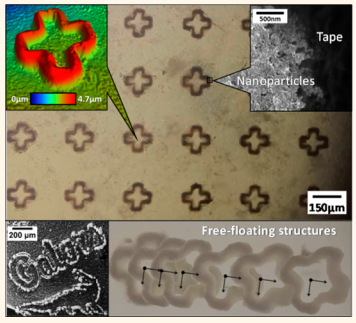

KEYWORDS: ferromagnetic materials microstructures · nanoparticles · particle deposition · self-assembly

Magnetically directed and self-assembly of magnetic micro/nanoparticles in one, two, and three dimensions[1] is of increasing interest owing to the unique stimuli-responsive behavior of the resultant micro/nanostructures. For example, in sensors and electronics,[2] assembly of magnetic nanoparticles into microstructures is desirable to tailor the properties of the structure (*e.g.*, photoelectrical activity,[3] surface morphology,[4] electrochemical response,[5] surface-enhanced Raman scattering,[6] or surface plasmons[7]). For microelectromechanical systems (MEMS),[8] structural characteristics of the assembled microstructures and the mechanical deformation of the structures in the presence of magnetic fields can be used for manipulation and actuation. In the biomedical field, there is interest in microstructures fabricated with magnetic nanoparticles for targeted delivery of therapeutic agents and for more effective diagnosis techniques that extend the limits of molecular diagnostics.[9] Magnetic nanoparticle assembly has also been used in photonics for obtaining periodic structures, designed to have a strong interactions with light.[10,11]

In the above examples, externally applied magnetic fields are used to drive the assembly of the particles. Methods for magnetically directed assembly can be generally classified as colloidal-assembly techniques and surface-patterning techniques. In the former, magnetic dipole−dipole interactions are used to drive the assembly of particles (typically microparticles) in suspension, while in the latter, magnetic media with a predetermined field gradient pattern is used to drive assembly of particles (typically nanoparticles) onto a surface.

The formation of magnetically directed colloidal superstructures with multipole symmetry, consisting of paramagnetic and diamagnetic microparticles assembled mediated by induced dipole−dipole interactions in a magnetic nanoparticle suspension, has been demonstrated.[12] Depending on the relative sizes and induced dipole moments of the constituent particles, a variety of shapes have also been demonstrated.[13−15] However, it is not possible to generate complex asymmetric shapes using this approach, and the structures reported thus far do not retain their shape once the magnetic field is removed,[16] except when fixing

* Address correspondence to carlos.rinaldi@bme.ufl.edu, darnold@ufl.edu.

Received for review June 22, 2015 and accepted September 12, 2015.

Published online September 12, 2015
10.1021/acsnano.5b03783

them to the substrate. Magnetic dipole−dipole interactions have also been used to drive the colloidal assembly of superparamagnetic microparticles into chain-like structures.[17,18] Cross-linking of the microparticles using complementary DNA strand hybridization and by chemical means has been reported to yield microparticle chains that retain their form once the magnetic field is removed.[19] These structures can also be manipulated using applied magnetic fields, in order to actuate their rotation and vibration,[18] and applications in mixing of microfluidic systems have been reported.[20] However, this method of magnetically directed assembly and cross-linking appears limited to formation of linear structures and lacks control over the length of the resulting linear aggregates. Thus, it would seem that current methods of colloidal magnetically directed assembly are limited to particles with a high degree of symmetry or to chain-like aggregates, and the current methods are difficult to extend to obtaining structures with complex asymmetric shapes.

For more complex shapes, the use of patterned magnetic media templates to drive the assembly of magnetic particles from solution to the surface of the media has also been reported. Experiments have demonstrated assemblies with micro-[21] and submicrometer feature sizes,[22−26] and simulations have indicated that assembly for such small structures occurs in millisecond time scales.[27,28] Most commonly, a magnetic pattern is recorded in magnetic recording media (*e.g.*, magnetic tape or a hard drive surface) using a magnetic write head.[29] The resulting magnetization pattern then generates magnetic field gradients that capture particles from solution, resulting in linear or bit-like patterns.[30] These patterns can be transferred to a polymer film substrate, which can be lifted off and used, for example, as a diffraction grating.[31] Although these techniques are promising, to date the complexity of the patterns of assembled magnetic particles has generally been limited to the geometry of the magnetic bit of the respective recording medium.[31] Furthermore, although basic shapes can be obtained using this method, they are confined to a surface or film, and fabrication of free-floating magnetic microstructures has not been demonstrated using these techniques.

In this contribution, we report a method that combines the potential of magnetically directed assembly of magnetic nanoparticles on a substrate with *in situ* nanoparticle cross-linking to obtain releasable free-floating complex magnetic microstructures. The magnetic field gradient patterns required to drive magnetic nanoparticle assembly into complex shapes are obtained using a selective magnetization technique to imprint relatively arbitrary magnetic pole patterns onto hard magnetic substrates using soft magnetic "magnetization masks".[32] By chemical cross-linking, the magnetically assembled structures retain their shape after release from the substrate even in the absence of a magnetic field. They can also be manipulated through applied magnetic stimulus, enabling control of their translational and rotational motion in suspension and their deformation, depending on their shape and degree of cross-linking. By changing the polymer linkers in combination with selected drug molecules a magnetically triggered drug release mechanism can be envisioned, as reported recently.[24,33−37] The reported method is a simple, low-cost, and scalable route to generating free-floating magnetically assembled complex microstructures of cross-linked magnetic nanoparticles. Furthermore, refinement of the selective magnetization and cross-linking steps should enable generating structures with submicrometer features. Finally, the process flow could conceivably be adapted for continuous, *e.g.*, roll-to-roll, fabrication of the magnetic microstructures.

RESULTS AND DISCUSSION

The fabrication method of magnetic microstructures is illustrated schematically in Figure 1, where magnetic nanoparticles are assembled *via* the magnetic fields from a magnetically patterned substrate (in this case a Hi8MP video cassette tape). The particles preferentially assemble in the higher magnetic gradient regions at the boundaries of the magnetic poles, allowing for the generation of complex two-dimensional shapes.

Both iron oxide (Fe_3O_4) and cobalt ferrite ($CoFe_2O_4$) nanoparticles were used in this work, in an effort to explore how different magnetic relaxation mechanisms may influence the assembly process.[11,17,38,39] During the assembly process, particles will translate and rotate as they respond to the magnetic field gradient generated by the magnetic pole pattern. The iron oxide nanoparticles used in this study respond to magnetic fields through internal dipole rotation, known as Néel relaxation, whereas the cobalt ferrite nanoparticles used in this study respond to magnetic fields by rigid body rotation, known as Brownian relaxation. We expected possible differences in the rate of assembly of the Néel and Brownian particles due to the differences in magnetic torques and the corresponding hydrodynamic translation/rotation coupling. However, as will be seen upon discussion of our results, there were no measurable differences in the assembly rates of the two types of nanoparticle.

The iron oxide and cobalt ferrite nanoparticles were each synthesized by thermal decomposition.[40,41] The hydrodynamic diameter distributions were obtained by dynamic light scattering (DLS) using a Brookhaven Instruments 90Plus/BIMAS. For the analysis, oleic acid-coated nanoparticles were suspended in toluene and then filtered with 0.1 mm PTFE filter syringes prior to measurement. Typical number-weighted hydrodynamic diameters for the oleic acid-coated particles used in the experiments were 19 ± 3.9 nm for iron oxide and 20 ± 3.3 nm for cobalt ferrite (see Figure S1).

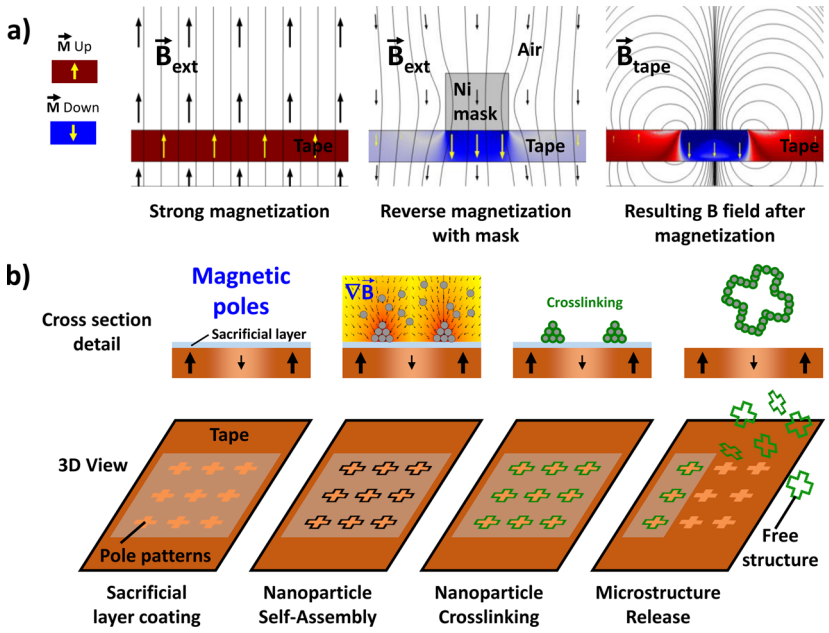

Figure 1. Schematic of fabrication process: (a) (From left) Selective magnetization. Magnetic tape is strongly magnetized up (6 T). Then the nickel mask is placed on top of the tape, and a reverse magnetic field is applied (200 mT). This reversal field selectively reverses the direction of the magnetization on the tape only in the areas underneath the mask. (b) (From left) Coating of the selective magnetized tape with a sacrifical layer. Magnetic assembly of the particles over the magnetic patterns. Cross-linking of nanoparticles on the substrate with PEI. Dissolution of the sacrificial layer and releasing of magnetic structures.

The particle's core diameter distribution was determined by fitting the diameter histograms measured by transmission electron microscope (TEM) (JEOL 200CX microscope, operating at 120 kV acceleration voltage) to a log-normal size distribution (see Figure S1), indicating the particles had narrow size distributions, with average core diameters of 17 ± 5.6 nm for iron oxide and 13 ± 2.9 nm for cobalt ferrite.

Some of the iron oxide nanoparticles were transferred to the aqueous phase by cleavage of the oleic acid double bond to obtain nanoparticles with surface carboxylic acid groups. The resulting nanoparticles were now colloidally stable in aqueous media and possessed reactive carboxylic acid groups that were subsequently used to cross-link the structures. After transferring the particles to the aqueous phase, the particle hydrodynamic diameter remained practically the same (see Figure S7a), confirming that there was no particle aggregation.

Equilibrium magnetization measurements at 300 K for aqueous nanoparticle suspensions, made using an MPMS-3 superconducting quantum interference device (SQUID) magnetometer (Quantum Design), demonstrated superparamagnetic behavior (Figure S7c) in the samples. By fitting the data to the Langevin function using the procedure suggested by Chantrell,[42] the average magnetic diameter was 8 ± 5.2 nm for iron oxide and 13 ± 3.3 nm for cobalt ferrite, while the volume fractions (ϕ) of magnetic nanoparticles in the stock solutions were determined to be 0.19% and 0.14%, respectively. After transferring the iron oxide nanoparticles to the aqueous phase, the average magnetic diameter was 9 ± 4.5 nm, and the magnetic volume fraction (ϕ) in the stock solution was 0.062% (summarized characteristics of particles used in cross-linking experiment are presented in Supporting Information Table S3).

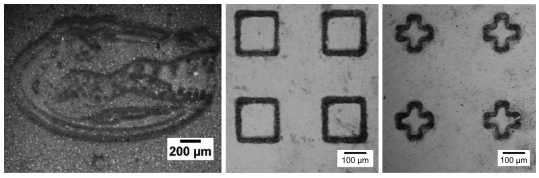

Figure 2. Magnetically assembled iron oxide nanoparticles and cross-linked microstructures over the magnetic tape substrate before release.

The poles in the magnetic tape were created by a selective magnetization technique using soft magnetic "magnetization masks".[43] A magnetization mask (hereafter mask) was fabricated by electroplating 45-μm-thick Ni structures on a silicon wafer. Different shape and size structures were included in the mask, as shown in Figure 2. However, detailed analysis focused on 175-μm-wide squares and 150-μm-wide crosses with a minimum edge-to-edge distance between structures of 225 μm. It is important to remark that the magnetic mask can be reused, thereby reducing fabrication time and cost associated with lithography steps. A magnetic reversal field of ~200 mT was used to generate the magnetization pattern in the magnetic tape substrate. Because experimental measurement of

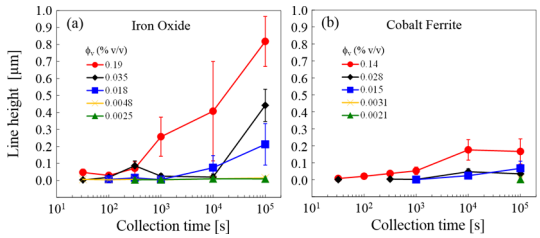

Figure 3. Time dependence of the line height for different volume fractions. (a) Iron oxide nanoparticles with Néel relaxation mechanism and (b) cobalt ferrite nanoparticles with Brownian relaxation mechanism.

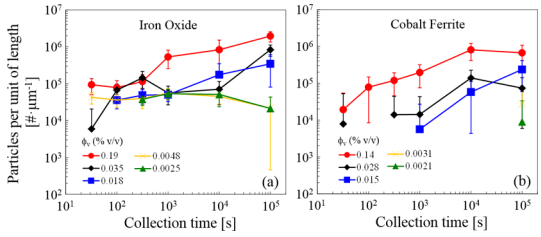

Figure 4. Calculation of number of particles per cross section *vs* time, parametric with the suspension's volume fraction for (a) iron oxide particles and (b) cobalt ferrite particles.

the resultant microscale magnetic field gradients is quite difficult, simulations[44] were used to estimate orders of magnitude of the magnetic field and magnetic field gradient in a typical boundary between two opposing magnetic poles (refer to measured magnetic properties of the tape in Figure S3 and simulation result in Figure S4).

The kinetics of the assembly process and the resultant microstructural features were studied for three process variables: (1) assembly time, (2) volume fraction of the particles in suspension, and (3) iron oxide *vs* cobalt ferrite nanoparticles. Figure 3 shows the average deposited line height as a function of time for different volume fractions and particle types. As expected, the line height increases with increasing collection time and increasing particle concentration. The line height is greater for the iron oxide particles (Figure 3a) as compared to the cobalt ferrite particles (Figure 3b) under all conditions tested. This observation was initially unexpected, considering that iron oxide exhibited a smaller magnetic core diameter than the cobalt ferrite (8 ± 5.2 nm *vs* 13 ± 3.3 nm). Because of their larger magnetic core diameter, the cobalt ferrite particles would experience a larger magnetic force during assembly. However, the two particles have unequal hydrodynamic diameters, so additional analysis was performed to estimate the number of particles collected (details provided in the Supporting Information).

Figure 4 shows the number of particles assembled per unit length as a function of assembly time for different volume fractions and particle types. The roughness of the substrate and the detection limits

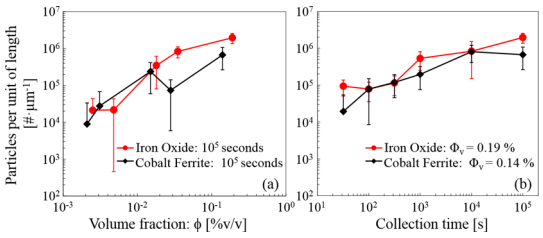

Figure 5. Number of particles per unit of length. (a) Volume fraction dependence (time = 10^5 s) and (b) time dependence (for cobalt ferrite ϕ = 0.14% and iron oxide ϕ = 0.19%).

of the profilometer caused significant statistical variation in the data. The most reliable results were generated by samples with larger numbers of particles accumulated on the substrate, *e.g.*, the experiments with maximum collection time (10^5 s) and maximum volume fractions of particles in solution (0.19% for iron oxide and 0.14% for cobalt ferrite). Figure 5 further illustrates these maximal cases for direct comparison between the two particle types. It is worth noting that the order of magnitude of number of particles collected is the same for both particle relaxation mechanisms. However, the iron oxide particles exhibit a larger line height because the core diameter is greater than the cobalt ferrite particles (17 nm *vs* 13 nm).

As was pointed out earlier, we expected possible differences in the rate of assembly of nanoparticles with Néel (iron oxide) *vs* Brownian (cobalt ferrite) relaxation mechanisms. However, the results of Figure 5 indicate that particles with either relaxation mechanism are captured at essentially the same rate. Consequently, it was decided to carry out subsequent experiments demonstrating cross-linking and release solely with the iron oxide nanoparticles.

To demonstrate fabrication of free-floating structures, an assembly experiment was conducted using the iron oxide nanoparticles that had been transferred to the aqueous phase (ϕ = 0.062%) and an assembly time of 19 h. The resulting structures had typical line heights and widths of 230 ± 80 nm and 3.9 ± 1 μm, respectively. After assembly, the carboxylic acid groups present on the nanoparticle surface were cross-linked with the primary amines present in branched polyethylenimine (PEI).[45−48] A schematic of the process from phase transfer to cross-linking is shown in Figure 6. Structure release was achieved by dissolving an underlying sacrificial layer of polydimethylglutarimide-based resist added before particle assembly. Figure 7 illustrates the results by showing free-floating structures and demonstrating the successful cross-linking of particles forming a structure. Figure S9 presents an additional TEM image of the free-floating structure, illustrating the entrapment of the cross-linked particles in the structure. Additional magnetic characterization of the resulting free-floating structures is presented in Figure S10, which demonstrates that structures have superparamagnetic properties

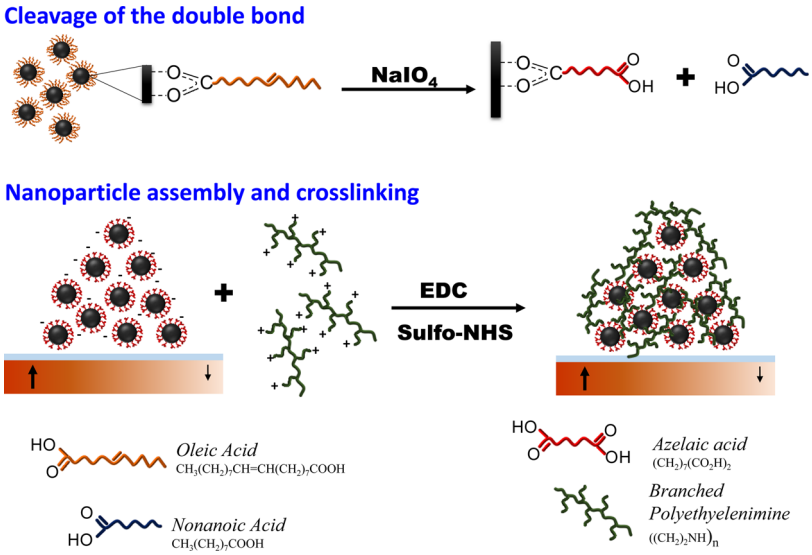

Figure 6. Schematic of the cross-linking process on iron oxide nanoparticles, starting from the formation of the oleic acid after particle thermal decomposition. The cleavage of the double bond in the oleic acid creates a terminal carboxylic group that can be used to cross-link particles using a polyamine such as PEI, *via* EDC chemistry.

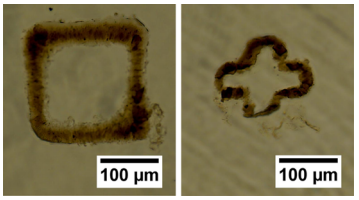

Figure 7. Examples of released structures free-floating in water after cross-linking iron oxide nanoparticles with 25 kDa PEI.

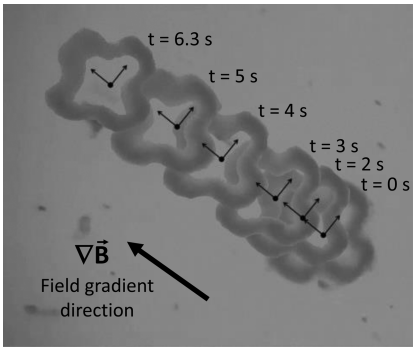

Figure 8. Superimposed snapshots of a single microstructure translated toward a magnetic field generated by a permanent magnet (images extracted from Video S2). Structure are made of iron oxide nanoparticles.

similar to those of the nanoparticles used in their formation. Superparamagnetic behavior is desirable because micrometric-size structures will be magnetized in the presence of external fields (higher susceptibility than counterpart paramagnetic structures), but structure agglomeration and unwanted structure–structure interaction in the absence of magnetic field will be prevented due to the absence of residual magnetization.

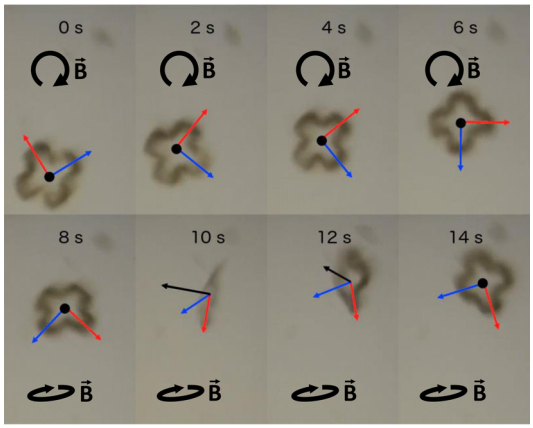

Figure 9. (Top) Rotation of a microstructure by rotating the magnetic field. (Bottom) Microstructure flipping produced by the change of direction of the rotation in the magnetic field (images extracted from Video S3). Structure are made of iron oxide nanoparticles.

The free-floating magnetic microstructures were shown to retain their geometric shape, even under response to an applied magnetic field. Figure 8 illustrates the displacement of one of those structures in the presence of an applied magnetic field generated by a permanent magnet. The displacement of the structure was in the direction of the higher field gradient, due to magnetic forces exerted on the magnetic nanoparticles within the structure.[49] In other experiments the direction of the applied magnetic field was changed, and the microstructures were shown to move along different axes (rotate and flip) depending on the direction of magnetic field rotation, as illustrated in Figure 9 (different motions of the structure are presented in Video S1 to Video S4). These observations demonstrate the potential utility of these structures that can be

remotely actuated and retain their shape after the magnetic field is removed.

CONCLUSIONS

A fabrication technique to obtain free-floating magnetic microstructures by *in situ* cross-linking of magnetically assembled nanoparticles was demonstrated. Complex two-dimensional geometric shapes were obtained by using a selective magnetization technique to define structure boundaries. Squares and crosses were obtained with external dimensions of 175 and 150 μm, respectively, with boundary line dimensions of 230 $\pm$ 80 nm in height and 3.9 $\pm$ 1 μm in width. The magnetic microstructures were successfully released from the substrate and retained their shape in suspension during manipulation with external magnetic fields.

EXPERIMENTAL METHODS

Substrate Magnetization. Using the methods described by Garraud *et al.*,[32] a nickel magnetization mask (hereafter the mask) is used to create the desired magnetic patterns (shapes) on a magnetic substrate (Hi8MP video cassette tape). The mask was optimized by simulating the magnetization process using the finite element method in COMSOL Multiphysics in order to minimize magnetic field interference between structures. Size, separation between structures, and mask thickness were simulated. To imprint the geometric shapes of the mask as magnetic pole patterns in the tape, a selective magnetization method reported by Oniku *et al.*[43] was used. In this method, first a tape is uniformly premagnetized out-of-plane (6 T, upward); then the mask is placed in contact with the tape to apply a reverse (downward) magnetic field pulse. Patterns were generated using reversal fields of 200 mT, which yielded the best results.

Nanoparticle Synthesis and Phase Transfer. Two different magnetic nanoparticles representing two different relaxation mechanisms were studied: iron oxide nanoparticles with predominant Néel relaxation mechanism (*i.e.*, magnetic dipole alignment with the applied field without physical particle rotation) and cobalt ferrite with predominant Brownian relaxation mechanism (*i.e.*, particle physical rotation due to magnetic dipole alignment).

Iron oxide nanoparticles were synthesized by thermal decomposition of an iron oleate precursor as described by Park *et al.*[40] An iron oleate was prepared by mixing sodium oleate (72 mmol) and iron(III) chloride hexahydrate in 3:1 molar ratio with water (36 mL), hexane (84 mL), and ethanol (48 mL). The mixture was kept at 70 °C for 4 h under reflux and further washed with water to remove unreacted reagents. Thermal decomposition of the iron oleate in a high-boiling-point solvent in the presence of oleic acid yielded iron oxide nanoparticles coated with a monolayer of oleic acid and narrow size distributions. Trioctylamine was used as the solvent, and the temperature was maintained at 345 °C for 1 h. After synthesis, magnetic nanoparticles were suspended in chloroform and precipitated with acetone to remove the excess of solvent and free oleic acid and finally dried at room temperature to remove excess solvent.

Cobalt ferrite nanoparticles with predominant Brownian relaxation mechanism were synthesized by thermal decomposition of organometallic precursor at 320 °C in the presence of oleic acid using 1-octadecene as solvent.[41] The iron/cobalt oleate was prepare using a 2:1 molar ratio of iron(III) chloride hexahydrate to cobalt(II) in a mixture of 50 mL of deionized water, 100 mL of hexane, and 50 mL of ethanol at 67 °C under reflux condenser during 4 h and then aged for 3 days. 1-Octadecene was used as the solvent, and the temperature was maintained at 320 °C for 3 h. After synthesis the reaction product was washed using the same procedure as for iron oxide nanoparticles.

The physical (Figure S1) and magnetic properties (Figure S2) of the iron oxide and cobalt ferrite nanoparticles and some characteristics of their suspensions are summarized in Table S1, and a detailed description of the methods to characterize these particles is provided in Section 1 of the Supporting Information.

The as-synthesized iron oxide and cobalt ferrite nanoparticles were soluble only in organic solvents due to oleic acid coating their surface. In order to cross-link the nanoparticles in their magnetically assembled patterns, a reactive group is necessary on the particle surface. Furthermore, most applications of interest require particles that are compatible with an aqueous environment. Therefore, a phase transfer procedure described by Wang *et al.*[50] was used to cleave the double bond in the oleic acid chain, simultaneously transferring the particles to the aqueous phase and introducing a reactive carboxylic acid group on the outer surface of the nanoparticles. In a typical procedure, dried particles (100 mg) were suspended in toluene (10 mL) and mixed with a mixture of ethyl acetate/acetonitrile, 1:1 volume ratio (8 mL), and a solution of sodium periodate (6 mL of 0.28 M $NaIO_4$). The mixture was placed under ultrasound for 20 min, and the product was magnetically decanted to remove excess solvent. For particle assembly over the magnetized substrate, a stock solution was prepared by suspending particles in water (10 mL). This procedure is equally effective for iron oxide and cobalt ferrite nanoparticles, although only the results for the iron oxide nanoparticles are reported herein.

Nanoparticle Assembly. The patterned substrate was immersed in a suspension of magnetic nanoparticles, and after a specified assembly time, the substrate was removed from the particle suspension, washed with water at the same pH of the particle solution, and dried at room temperature. Serial stock dilutions of 1:1, 1:5, 1:10, 1:50, and 1:100 were prepared in order to study the effect of nanoparticle volume fraction on the assembly process. Representative measured profiles of the particle collections for these concentrations are presented in Figure S6.

The volume fraction was calculated from the measured magnetization curve using SQUID. Table S2 provides a summary of the volume fractions for solutions considered in the experiments. Particles were collected over independent substrates (for different relaxation mechanism and different volume fraction), during 32, 100, 316, 1000, 10 000, and 100 000 s.

Analysis of Nanoparticle Assemblies. The microstructural features of the assembled structures were evaluated by optical profilometry measurements. An optical profilometer (Contour GT-I, Bruker) was used to measure the hill-like profile of the collected nanoparticles over the substrate, as shown in Figure S5a. Postprocessing analysis converted the 3D-profile map into a series of cross sections as shown in Figure S5b. From this, the average line widths (at the base of the hill) and average line heights were calculated for different experimental conditions. Each experimental condition was analyzed using cross sections from five different square microstructures. Using these averaged profiles it was possible to estimate the number of particles collected by unit of length as described in Section 2 of the Supporting Information.

Nanoparticle Cross-Linking. For the nanoparticle cross-linking, iron oxide nanoparticles in the water phase, described in section 4.2, were assembled for 19 h by immersing the tape in a particle suspension. Characteristics of particles in water phase are summarized in Table S3 in the Supporting Information. A gentle wash process with deionized water over the inclined surface was necessary after assembly to remove free particles from the surface. Once the particles were deposited, a solution of branched PEI (25 wt % and molecular weight of 2.5 kDa) was used to cross-link the carboxylic acid groups present on the nanoparticle surfaces with the primary amines in the polymer chains, using 1-ethyl-3-[3-(dimethylamino)propyl]carbodiimide hydrochloride (EDC) chemistry (0.03 mmol). To catalyze the reaction, *N*-hydroxysulfosuccinimide (Sulfo-NHS) was added to the solution at an EDC/Sulfo-NSH molar ratio of 0.1. The reaction

was carried out by adding this solution on top of the substrate containing magnetically assembled microstructures, and the reaction was allowed to occur for 1 h. A final rinse with deionized water and acetic acid was used to remove free polymer (process described in Figure 6). A TEM comparison of the particles before assembly and after deposition is presented in the Supporting Information Figure S8.

Structure Release. In order to release structures, the magnetizable tape was coated with a 350-nm-thick sacrificial layer of LOR 3B (polydimethylglutarimide-based resist), after the selective magnetization step. After magnetic assembly and cross-linking of nanoparticles on top of the sacrificial layer, this underlying sacrificial layer was dissolved in AZ300 MIF developer (tetramethylammonium hydroxide), releasing the magnetic microstructures into solution. Samples were very gently agitated to accelerate dissolution of the LOR 3B layer.

Conflict of Interest: The authors declare no competing financial interest.

Supporting Information Available: The Supporting Information is available free of charge on the ACS Publications website at DOI: 10.1021/acsnano.5b03783.

Details of the nanoparticle synthesis and characterization, simulations of the magnetic field patterns from the magnetic tape, mathematical procedures used to calculate the number of particles assembled from the experimental measurements, additional figures illustrating the cross-linking process, and magnetic measurements of the cross-linked microstructures (PDF)
Videos with examples of manipulation of free-floating micromagnetic structures in response to applied external magnetic fields (AVI)
Video (AVI)
Video (AVI)
Video (AVI)

Acknowledgment. This work was funded in part by the University of Florida Office of Research. The authors thank Dr. Alexandra Garraud, Oniku Ololade, and Nicolas Garraud for their contribution and the staff of the UF Nanoscale Research Facility and the UF Major Analytical Instrumentation Center for their assistance in the microfabrication and material characterization.

REFERENCES AND NOTES

1. Dai, Q.; Nelson, A. Magnetically-Responsive Self Assembled Composites. *Chem. Soc. Rev.* **2010**, *39*, 4057–4066.
2. Shipway, A. N.; Katz, E.; Willner, I. Nanoparticle Arrays on Surfaces for Electronic, Optical, and Sensor Applications. *ChemPhysChem* **2000**, *1*, 18–52.
3. Chirita, M.; Grozescu, I. Fe_2O_3 – Nanoparticles, Physical Properties and Their Photochemical and Photoelectrochemical Applications. *Chem. Bull. Politeh. Univ. Timsisoara* **2009**, *54*, 1–8.
4. Kouassi, G. K.; Irudayaraj, J. Magnetic and Gold-Coated Magnetic Nanoparticles As a DNA Sensor Magnetic and Gold-Coated Magnetic Nanoparticles As a DNA Sensor. *Anal. Chem.* **2006**, *78*, 3234–3241.
5. Qu, S.; Wang, J.; Kong, J.; Yang, P.; Chen, G. Magnetic Loading of Carbon Nanotube/nano-Fe3O4 Composite for Electrochemical Sensing. *Talanta* **2007**, *71*, 1096–1102.
6. Gong, J. L.; Liang, Y.; Huang, Y.; Chen, J. W.; Jiang, J. H.; Shen, G. L.; Yu, R. Q. Ag/SiO2 Core-Shell Nanoparticle-Based Surface-Enhanced Raman Probes for Immunoassay of Cancer Marker Using Silica-Coated Magnetic Nanoparticles As Separation Tools. *Biosens. Bioelectron.* **2007**, *22*, 1501–1507.
7. Wang, J.; Munir, A.; Zhu, Z.; Zhou, H. S. Magnetic Nanoparticle Enhanced Suface Plasmon Resonance Sensing and Its Application for the Ultrasensitive Detection of Magnetic Nanoparticle-Enriched Small Molecules. *Anal. Chem.* **2010**, *82*, 6782–6789.
8. Kim, J.; Chung, S. E.; Choi, S.-E.; Lee, H.; Kim, J.; Kwon, S. Programming Magnetic Anisotropy in Polymeric Microactuators. *Nat. Mater.* **2011**, *10*, 747–752.
9. Emerich, D. F.; Thanos, C. G. The Pinpoint Promise of Nanoparticle-Based Drug Delivery and Molecular Diagnosis. *Biomol. Eng.* **2006**, *23*, 171–184.
10. Yethiraj, A.; Thijssen, J. H. J.; Wouterse, A.; van Blaaderen, A. Large-Area Electric-Field-Induced Colloidal Single Crystals for Photonic Applications. *Adv. Mater.* **2004**, *16*, 596–600.
11. He, L.; Hu, Y.; Kim, H.; Ge, J.; Kwon, S.; Yin, Y. Magnetic Assembly of Nonmagnetic Particles into Photonic Crystal Structures. *Nano Lett.* **2010**, *10*, 4708–4714.
12. Yellen, B. B.; Friedman, G. Programmable Assembly of Heterogeneous Colloidal Particle Arrays. *Adv. Mater.* **2004**, *16*, 111–115.
13. Erb, R. M.; Son, H. S.; Samanta, B.; Rotello, V. M.; Yellen, B. B. Magnetic Assembly of Colloidal Superstructures with Multipole Symmetry. *Nature* **2009**, *457*, 999–1002.
14. Yang, Y.; Gao, L.; Lopez, G. P.; Yellen, B. B. Tunable Assembly of Colloidal Crystal Alloys Using Magnetic Nanoparticle Fluids. *ACS Nano* **2013**, *7*, 2705–2716.
15. Wang, M.; He, L.; Yin, Y. Magnetic Field Guided Colloidal Assembly. *Mater. Today* **2013**, *16*, 110–116.
16. Demirörs, A. F.; Pillai, P. P.; Kowalczyk, B.; Grzybowski, B. a. Colloidal Assembly Directed by Virtual Magnetic Moulds. *Nature* **2013**, *503*, 99–103.
17. Biswal, S.; Gast, A. Mechanics of Semiflexible Chains Formed by Poly(ethylene Glycol)-Linked Paramagnetic Particles. *Phys. Rev. E: Stat. Phys., Plasmas, Fluids, Relat. Interdiscip. Top.* **2003**, *68*, 021402.
18. Biswal, S. L.; Gast, A. P. Rotational Dynamics of Semiflexible Paramagnetic Particle Chains. *Phys. Rev. E. Stat. Nonlin. Soft Matter Phys.* **2004**, *69*, 041406.
19. Li, D.; Banon, S.; Biswal, S. L. Bending Dynamics of DNA-Linked Colloidal Particle Chains. *Soft Matter* **2010**, *6*, 4197.
20. Biswal, S. L.; Gast, A. P. Micromixing with Linked Chains of Paramagnetic Particles. *Anal. Chem.* **2004**, *76*, 6448–6455.
21. Zanini, L. F.; Dempsey, N. M.; Givord, D.; Reyne, G.; Dumas-Bouchiat, F. Autonomous Micro-Magnet Based Systems for Highly Efficient Magnetic Separation. *Appl. Phys. Lett.* **2011**, *99*, 232504.
22. Yellen, B. B.; Hovorka, O.; Friedman, G. Arranging Matter by Magnetic Nanoparticle Assemblers. *Proc. Natl. Acad. Sci. U. S. A.* **2005**, *102*, 8860–8864.
23. Sahoo, Y.; Cheon, M.; Wang, S.; Luo, H.; Furlani, E. P.; Prasad, P. N. Field-Directed Self-Assembly of Magnetic Nanoparticles. *J. Phys. Chem. B* **2004**, *108*, 3380–3383.
24. Singamaneni, S.; Bliznyuk, V. N.; Binek, C.; Tsymbal, E. Y. Magnetic Nanoparticles: Recent Advances in Synthesis, Self-Assembly and Applications. *J. Mater. Chem.* **2011**, *21*, 16819.
25. He, L.; Hu, Y.; Han, X.; Lu, Y.; Lu, Z.; Yin, Y. Assembly and Photonic Properties of Superparamagnetic Colloids in Complex Magnetic Fields. *Langmuir* **2011**, *27*, 13444–13450.
26. Kruglova, O.; Demeyer, P.-J.; Zhong, K.; Zhou, Y.; Clays, K. Wonders of Colloidal Assembly. *Soft Matter* **2013**, *9*, 9072.
27. Xue, X.; Furlani, E. P. Template-Assisted Nano-Patterning of Magnetic Core-Shell Particles in Gradient Fields. *Phys. Chem. Chem. Phys.* **2014**, *16*, 13306–13317.
28. Xue, X.; Furlani, E. P. Analysis of the Dynamics of Magnetic Core−Shell Nanoparticles and Self-Assembly of Crystalline Superstructures in Gradient Fields. *J. Phys. Chem. C* **2015**, *119*, 5714–5726.
29. Henderson, J.; Shi, S.; Cakmaktepe, S.; Crawford, T. M. Pattern Transfer Nanomanufacturing Using Magnetic Recording for Programmed Nanoparticle Assembly. *Nanotechnology* **2012**, *23*, 185304.
30. Ye, L.; Qi, B.; Pearson, T.; Cordeau, Y.; Mefford, O. T.; Crawford, T. M. Real Time Monitoring of Superparamagnetic Nanoparticle Self-Assembly on Surfaces of Magnetic Recording Media. *J. Appl. Phys.* **2014**, *115*, 17B513.
31. Ye, L.; Terry, B.; Mefford, O. T.; Rinaldi, C.; Crawford, T. M. All-Nanoparticle Concave Diffraction Grating Fabricated by Self-Assembly onto Magnetically-Recorded Templates. *Opt. Express* **2013**, *21*, 1994–1998.
32. Garraud, A.; Oniku, O. D.; Patterson, W. C.; Shorman, E.; Le Roy, D.; Dempsey, N. M.; Arnold, D. P. Microscale Magnetic

Patterning of Hard Magnetic Films Using Microfabricated Magnetizing Masks. In *MEMS 2014*; San Francisco, **2014**; pp 520−523.
33. Pankhurst, Q. A.; Connolly, J.; Jones, S. K.; Dobson, J. Applications of Magnetic Nanoparticles in Biomedicine. *J. Phys. D: Appl. Phys.* **2003**, *36*, R167–R181.
34. Dobson, J. Magnetic Nanoparticles for Drug Delivery. *Drug Dev. Res.* **2006**, *67*, 55–66.
35. Hoare, T.; Timko, B. P.; Santamaria, J.; Goya, G. F.; Irusta, S.; Lau, S.; Stefanescu, C. F.; Lin, D.; Langer, R.; Kohane, D. S. Magnetically Triggered Nanocomposite Membranes: A Versatile Platform for Triggered Drug Release. *Nano Lett.* **2011**, *11*, 1395–1400.
36. Sun, C.; Lee, J. S. H.; Zhang, M. Magnetic Nanoparticles in MR Imaging and Drug Delivery. *Adv. Drug Delivery Rev.* **2008**, *60*, 1252–1265.
37. Brazel, C. S. Magnetothermally-Responsive Nanomaterials: Combining Magnetic Nanostructures and Thermally-Sensitive Polymers for Triggered Drug Release. *Pharm. Res.* **2009**, *26*, 644–656.
38. Torres-Diaz, I.; Cortes, a; Cedeño-Mattei, Y.; Perales-Perez, O.; Rinaldi, C. Flows and Torques in Brownian Ferrofluids Subjected to Rotating Uniform Magnetic Fields in a Cylindrical and Annular Geometry. *Phys. Fluids* **2014**, *26*, 12004.
39. Min, Y.; Akbulut, M.; Kristiansen, K.; Golan, Y.; Israelachvili, J. The Role of Interparticle and External Forces in Nanoparticle Assembly. *Nat. Mater.* **2008**, *7*, 527–538.
40. Park, J.; An, K.; Hwang, Y.; Park, J.-G.; Noh, H.-J.; Kim, J.-Y.; Park, J.-H.; Hwang, N.-M.; Hyeon, T. Ultra-Large-Scale Syntheses of Monodisperse Nanocrystals. *Nat. Mater.* **2004**, *3*, 891–895.
41. Herrera, A. P.; Polo-Corrales, L.; Chavez, E.; Cabarcas-Bolivar, J.; Uwakweh, O. N. C.; Rinaldi, C. Influence of Aging Time of Oleate Precursor on the Magnetic Relaxation of Cobalt Ferrite Nanoparticles Synthesized by the Thermal Decomposition Method. *J. Magn. Magn. Mater.* **2013**, *328*, 41–52.
42. Chantrell, R.; Popplewell, J.; Charles, S. Measurements of Particle Size Distribution Parameters in Ferrofluids. *IEEE Trans. Magn.* **1978**, *14*, 975–977.
43. Oniku, O. D.; Ryiz, P. V.; Garraud, A.; Arnold, D. P. Imprinting of Fine-Scale Magnetic Patterns in Electroplated Hard Magnetic Films Using Magnetic Foil Masks. *J. Appl. Phys.* **2014**, *115*, 17A718.
44. Oniku, O. D.; Garraud, A.; Shorman, E.; Patterson, W. C.; Arnold, D. P. Modeling of a Micromagnetic Imprinting Process. In Tech. Dig. Solid-State Sensors, Actuators, and Microsystems Workshop (Hilton Head 2014); Hilton Head Island, South Carolina, 2014, pp 187−190.
45. López-Cruz, A.; Barrera, C.; Calero-DdelC, V. L.; Rinaldi, C. Water Dispersible Iron Oxide Nanoparticles Coated with Covalently Linked Chitosan. *J. Mater. Chem.* **2009**, *19*, 6870.
46. Wang, X.; Zhou, L.; Ma, Y.; Li, X.; Gu, H. Control of Aggregate Size of Polyethyleneimine-Coated Magnetic Nanoparticles for Magnetofection. *Nano Res.* **2009**, *2*, 365–372.
47. Yiu, H. H. P.; McBain, S. C.; Lethbridge, Z. A. D.; Lees, M. R.; Dobson, J. Preparation and Characterization of Polyethylenimine-Coated Fe3O4-MCM-48 Nanocomposite Particles As a Novel Agent for Magnet-Assisted Transfection. *J. Biomed. Mater. Res., Part A* **2010**, *92*, 386–392.
48. Madison, S. A.; Carnali, J. O. pH Optimization of Amidation via Carbodiimides. *Ind. Eng. Chem. Res.* **2013**, *52*, 13547–13555.
49. Varón, M.; Beleggia, M.; Kasama, T.; Harrison, R. J.; Dunin-Borkowski, R. E.; Puntes, V. F.; Frandsen, C. Dipolar Magnetism in Ordered and Disordered Low-Dimensional Nanoparticle Assemblies. *Sci. Rep.* **2013**, *3*, 1234.
50. Wang, M.; Peng, M.-L.; Cheng, W.; Cui, Y.-L.; Chen, C. A Novel Approach for Transfering Oleic Acid Capped Iron Oxide Nanoparticles to Water Phase. *J. Nanosci. Nanotechnol.* **2011**, *11*, 3688–3691.